A Local Boundary Integral Equation (LBIE) Method in 2D Electromagnetic Wave Scattering, and a Meshless Discretization Approach

Williams L. Nicomedes, Renato C. Mesquita* and Fernando J. S. Moreira
Dept. of Electronics Engineering and *Dept. of Electrical Engineering
Federal University of Minas Gerais (UFMG), Belo Horizonte, Brazil
wlnicomedes@yahoo.com.br; renato@ufmg.br; fernandomoreira@ufmg.br

***Abstract*— In this work, we apply the Local Boundary Integral Equation (LBIE) Method to the scattering problem of a plane wave by a dielectric cylinder. This method together with a meshless discretization approach, known as *meshless*, provides very accurate results, when compared to analytical solutions. The method is an efficient tool in electromagnetic scattering analysis because among its principal characteristics, it is based on local interactions, thus leading to a sparse matrix.**

Keywords - Meshless; LBIE; MLPG4; Scattering; RBC

I. INTRODUCTION

Meshless methods are relatively new; only recently they have been applied as a tool for numerical solutions in engineering. The first applications concerning them can be traced to the early past decade [1]. The meshless approach is still in development; one could say that it is on its infancy, with many challenging problems that remain to be solved [1].

The family of meshless methods is intended to be an alternative to the Finite Element Method (FEM). As it is well known, FEM requires a mesh, or a grid with connectivity between the elements, which sometimes demonstrates to be a strong shortcoming. Meshless methods, otherwise, require no mesh; nodes are simply spread over the domain, and no connectivity among them is demanded. This makes them very attractive because they work on the same grounds as FEM in what concerns local interactions (sparse matrices) and have no need for any mesh.

Meshless methods have successfully been applied in Mechanics, mainly in Elastostatics and Hydrodynamics. In Electromagnetics, they have been applied in Electrostatics [2], low frequency [3] and high frequency problems [4]. In these previous works, a formulation known as Element Free Galerkin (EFG) has been used. EFG is not truly a meshless method, because a background mesh is necessary to perform numerical integration [1]. Another approach is provided by the Meshless Local Petrov Galerkin Method (MLPG) [5]. MLPG is a true meshless method, where no kind of mesh is necessary. Our approach is to use an integral formulation (in fact, a local boundary integral equation) and to discretize it using the MLPG. This formulation is applied to the scattering problem of a plane wave by an homogeneous dielectric cylinder; we could then compare the numerical results with the analytical solution, observing an excellent agreement between them.

II. THE LOCAL BOUNDARY INTEGRAL EQUATION FOR SCATTERING PROBLEMS

A. The Scenario

Considering a plane domain Ω with boundary Γ, we seek for the solutions of the Helmholtz equation (1) for nonmagnetic media inside this domain (magnetic permeability $\mu_r = 1$ everywhere). For a TM^z incident plane wave, the total field has only a $\hat{z}$-component, E_z:

$$\nabla^2 E_z + k^2 \varepsilon_r E_z = 0 \tag{1}$$

where $k = 2\pi/\lambda$ is the wavenumber and ε_r is the relative electric permeability (which could be a function of position). Given a point $\vec{x}_i$ inside the domain (for example, the point X in Fig. 1) we then take a test function u centered at $\vec{x}_i$, so that it satisfies (δ is the Dirac delta function):

$$\nabla^2 u = -\delta(\vec{x} - \vec{x}_i) \tag{2}$$

Its solution is known to be:

$$u(\vec{x}; \vec{x}_i) = \frac{1}{2\pi} ln\left(\frac{1}{r}\right) \tag{3}$$

where $r = \sqrt{(x - x_i)^2 + (y - y_i)^2}$ and (x_i, y_i) are the coordinates of point $\vec{x}_i$.

Applying to E_z and u the second Green's identity, we get:

$$-\alpha(\vec{x}_i)E_z(\vec{x}_i) + \iint_\Omega k^2 \varepsilon_r u E_z \, dS = \oint_\Gamma E_z \frac{\partial u}{\partial n} dl - \oint_\Gamma u \frac{\partial E_z}{\partial n} dl \tag{4}$$

The surface integral is to be evaluated at the entire domain Ω and the line integral at the global boundary Γ. The factor α arises in the integration of the delta function. It is equal to 1 for every $\vec{x}_i$ inside the domain; however, if $\vec{x}_i$ is exactly at the global boundary Γ, then α is proportional to the internal angle at $\vec{x}_i$ (for example, were $\vec{x}_i$ to be located at the corner of a square, α would be $1/4$; were it to be located at wedge with

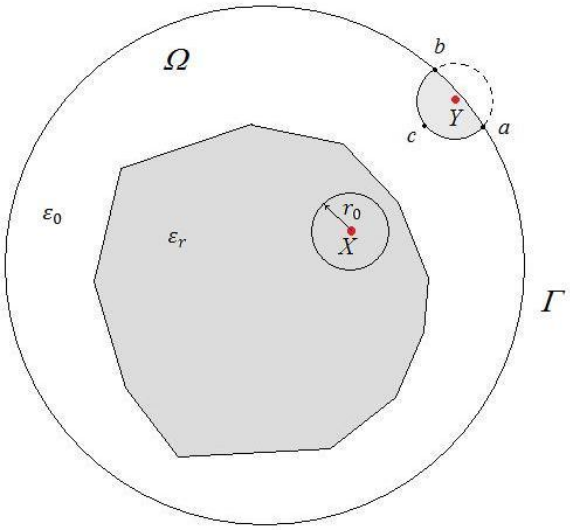

Figure 1. The problem domain Ω and the global boundary Γ. The irregular shaded area is the scatterer cross-section, characterized by a relative permittivity ε_r. X and Y are points at which E_z shall be calculated. X is an interior point, with a circular subdomain of radius r_0. Although Y is also an interior point, its subdomain intersects the global boundary, resulting in a noncircular local boundary (shaded area).

internal angle equal to θ radians, α would be $\theta/2\pi$). For a circular boundary, α is approximately equal to $1/2$. Because the line integrals are evaluated at the global boundary Γ, E_z and $\partial E_z/\partial n$ are respectively the Dirichlet and Neumann conditions prescribed at the global boundary Γ.

If, instead of integrating at the entire domain, we consider the integrations only at a local subdomain Ω_s (boundary Γ_s) around the point $\vec{x}_i$ [5] (small circle around X at Fig.1), expression (4) still holds, but E_z and $\partial E_z/\partial n$are no longer the known Dirichlet and Neumann conditions. So there are two unknowns at the local subdomain boundary, E_z and its normal derivative $\partial E_z/\partial n$. To avoid at least one of them, we arrange so that $\partial E_z/\partial n$ does not appear in (4), through the use of a slightly different test function u^* that goes to zero at the local boundary. If the subdomain is a circular one with radius r_0, then u^* is

$$u^* = u^*(\vec{x};\vec{x}_i) = \frac{1}{2\pi}\, ln\left(\frac{r_0}{r}\right) \tag{5}$$

So (4) becomes

$$-\alpha(\vec{x}_i)E_z(\vec{x}_i) + \iint_{\Omega_s} k^2\varepsilon_r u^* E_z dS = \oint_{\Gamma_s} E_z\frac{\partial u^*}{\partial n}dl - \oint_{\Gamma_s} u^*\frac{\partial E_z}{\partial n}dl \tag{6}$$

The line integrals in (6) shall be evaluated at the local boundary, a circle located $r_0$away from $\vec{x}_i$. For points whose local domains don't intersect the global boundary Γ (like X in Fig. 1), the last line integral in (6) does not need to be carried out. But for points like Y (Fig. 1), whose local domains are not circular, but a intersection between two circles, u^* is no longer zero in that portion that corresponds to the global boundary Γ (the dashed line is not a part of the local domain, only the shaded part). Taking the line integrals in (6), and considering their closed contour (local boundary) as a sum of two paths, one called *internal boundary* (ib), that is a line integral along the path acb and the other called *global boundary* (gb), that is a line integral along path ab, there follows:

$$-\alpha(\vec{x}_i)E_z(\vec{x}_i) + \iint_{\Omega_s} k^2\varepsilon_r u^* E_z dS = \int_{ib} E_z\frac{\partial u^*}{\partial n}dl + \int_{gb} E_z\frac{\partial u^*}{\partial n}dl - \int_{ib} u^*\frac{\partial E_z}{\partial n}dl - \int_{gb} u^*\frac{\partial E_z}{\partial n}dl \tag{7}$$

The third line integral is zero, because it depends on u^* evaluated at a distance $r = r_0$from $\vec{x}_i$. So we obtain:

$$-\alpha(\vec{x}_i)E_z(\vec{x}_i) + \iint_{\Omega_s} k^2\varepsilon_r u^* E_z dS = \int_{ib} E_z\frac{\partial u^*}{\partial n}dl + \int_{gb} E_z\frac{\partial u^*}{\partial n}dl - \int_{gb} u^*\frac{\partial E_z}{\partial n}dl \tag{8}$$

This is the local integral equation that must be satisfied for every point $\vec{x}_i$ in the domain. If $\vec{x}_i$ is an interior point whose local boundary does not intersect the global boundary (X in Fig. 1), there is no integration along a path like ab, and the terms which depend on gb are discarded. Thus (8) becomes equivalent to (6), where the last integral line it discarded, because it should be evaluated at a distance $r = r_0$ from $\vec{x}_i$.

B. Radiation Boundary Conditions

As could be seen, in (8) there is no information about the incident field E_z^{inc}; besides that, in the last line integral there is no prescribed condition on $\partial E_z/\partial n$. A kind of radiation boundary condition (RBC) has to be employed, to provide a link between the missing information.

RBC's are imposed in a contour located a certain distance away from the scatterer. In Fig. 1, the irregular shaded area represents the cross-section of the scatterer, which is composed of a dielectric material with relative permittivity ε_r. The circular line corresponding to the global boundary Γ is the contour along which RBC shall be imposed. It is seen that the global boundary comprises a certain space of the exterior medium (ε_0) surrounding the scatterer.

RBC's are needed because the differential formulation (from the Helmholtz differential equation, known as strong form, to equation (8), which is known as weak form) is not able to distinguish between outward-looking and inward looking solutions. Strictly speaking, when a scattering problem is solved through (8), there is no means to distinguish between the two linearly independent solutions which represent waves coming onto the scatterer (like those represented by the zero-order Hankel functions of the first type in analytical solutions, $H_0^{(1)}$) and going away from the scatterer (represented by Hankel functions of the second type, $H_0^{(2)}$). In other words, RBC's simulate the Sommerfeld boundary conditions:

$$\lim_{\rho\to\infty}\frac{\partial E_z^s}{\partial n} = -jkE_z^s \tag{9}$$

where E_z^s is the scattered field.

As discussed in [6], RBC's can be exact, i.e., they simulate (9) exactly in a finite radius. But this approach is nonlocal; the normal derivative of the field at one point of the global boundary depends on an integral of the tangential field along the whole boundary. When exact RBC's are imposed at a finite distance, the aforementioned integral leads to fully populated matrices, thus making no sense in using them. To overcome this problem, a number of *approximate* RBC's were developed in the past. One of them is the second-order Bayliss-Turkel RBC, suited for circular global boundaries. The Bayliss-Turkel conditions are obtained from an asymptotic expansion of the scattered field E_z^s [6]. Using polar coordinates (ρ, φ) to locate a point at the boundary, they are

$$\frac{\partial E_z^s}{\partial n} = \frac{\partial E_z^s}{\partial \rho} = \beta_1(\rho)E_z^s + \beta_2(\rho)\frac{\partial^2 E_z^s}{\partial \phi^2} \tag{10}$$

where coefficients β_1 and β_2 are given in terms of the finite boundary radius:

$$\beta_1(\rho) = \frac{-jk - \frac{3}{2\rho} + \frac{j3}{8k\rho^2}}{1 - \frac{j}{k\rho}} \tag{11}$$

and

$$\beta_2(\rho) = \frac{\frac{-j}{2k\rho^2}}{1 - \frac{j}{k\rho}} \tag{12}$$

Adding the term $\partial E_z^{inc}/\partial\rho$at both sides of (10):

$$\frac{\partial E_z^s}{\partial n} + \frac{\partial E_z^{inc}}{\partial n} = \beta_1(\rho)E_z^s + \beta_2(\rho)\frac{\partial^2 E_z^s}{\partial \phi^2} + \frac{\partial E_z^{inc}}{\partial n} \tag{13}$$

Noting that E_z is the sum of the incident and scattered fields (left side), adding and subtracting the following term at the right side

$$\beta_1(\rho)E_z^{inc} + \beta_2(\rho)\frac{\partial^2 E_z^{inc}}{\partial \phi^2} \tag{14}$$

there follows

$$\frac{\partial E_z}{\partial n} = \beta_1(\rho)E_z + \beta_2(\rho)\frac{\partial^2 E_z}{\partial \phi^2} + f(E_z^{inc}) \tag{15}$$

where $f(E_z^{inc})$ is a function of the incident field:

$$f(E_z^{inc}) = \frac{\partial E_z^{inc}}{\partial n} - \beta_1(\rho)E_z^{inc} - \beta_2(\rho)\frac{\partial^2 E_z^{inc}}{\partial \phi^2} \tag{16}$$

Substituting (15) in (8):

$$-\alpha(\vec{x}_i)E_z(\vec{x}_i) + \iint_{\Omega_s} k^2\varepsilon_r u^* E_z dS = \tag{17}$$

$$= \int_{ib} E_z\frac{\partial u^*}{\partial n}dl + \int_{gb} E_z\frac{\partial u^*}{\partial n}dl - \int_{gb} u^*\left[\beta_1(\rho)E_z + \beta_2(\rho)\frac{\partial^2 E_z}{\partial \phi^2}\right]dl - \int_{gb} u^* f(E_z^{inc})dl$$

This expression can be further simplified; the second derivative with respect to ϕ can be replaced by a simpler term. As the line integral in which it figures is evaluated along a portion of the global boundary where the radius ρ is a constant, all terms are functions of the ϕ solely. After some manipulations, that involve integration by parts, and reorganizing (17), we get the final expression:

$$\alpha(\vec{x}_i)E_z(\vec{x}_i) - \iint_{\Omega_s} k^2\varepsilon_r u^* E_z dS + \tag{18}$$
$$+ \int_{gb}\left[E_z\frac{\partial u^*}{\partial n} - \beta_1 u^* E_z + \beta_2\frac{\partial E_z}{\partial \phi}\frac{\partial u^*}{\partial \phi}\right]dl + \int_{ib} E_z\frac{\partial u^*}{\partial n}dl = \int_{gb} u^* f(E_z^{inc})dl$$

For a plane wave coming from the left,

$$E_z^{inc}(x,y) = e^{-jkx} \rightarrow E_z^{inc}(\rho,\phi) = e^{-jk\rho\,\cos\phi} \tag{19}$$

expression (16) becomes:

$$f(E_z^{inc}) = -[\beta_1 + (1+\beta_2\rho)jk\cos\phi - \beta_2 k^2\rho^2 sen^2\phi]e^{-jk\rho\,\cos\phi} \tag{20}$$

Expressions (18) and (20) form the LBIE with the second-order Bayliss-Turkel RBC embedded.

III. THE MESHLESS APPROACH

The meshless approach begins by spreading nodes over the domain of the problem to be solved. Nodes are simple points and to each one a *shape function* is associated. Each shape function has the property of being zero over the whole domain, except in the vicinity of the corresponding node. The vicinal region in which the shape function is different from zero is the node's *influence domain* [1]. The main difference between meshless methods and mesh-based methods (like FEM) is that the *element* concept is not present. The influence domains are arbitrary (the only restriction is that the set of influence domains must cover the entire domain) and can overlap. So, the nodes can be distributed arbitrarily without generating an element mesh.

For a given point (e.g. point $\vec{x} = X$ in Fig. 2), an unknown solution u is expressed as a sum of the contributions of those nodes that influence X, i.e. nodes that extend their influence domains onto X (they are depicted inside the circular shaded region):

$$u(\vec{x}) \sim u^h(\vec{x}) = \sum_{i=1}^{N}\phi_i(\vec{x})\hat{u}_i = \boldsymbol{\Phi}(\vec{x})\boldsymbol{u} \tag{21}$$

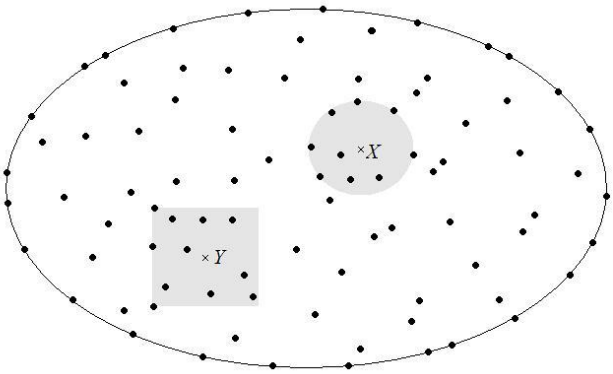

Figure 2. Nodes spread in a general domain. Those ones that influence points X and Y are shown as belonging to regions that surround these points (shaded regions).

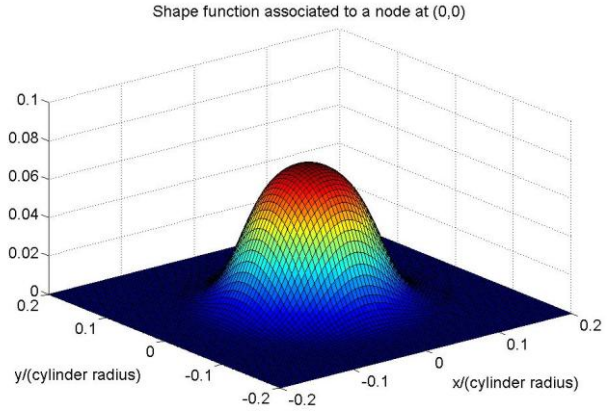

Figure 3. A MLS shape function located at the origin. Coordinates x and y are normalized with respect to the cylinder radius.

where u^h is the approximated solution, N is the number of nodes whose influence domains include the point $\vec{x}$, each ϕ_i is the i-th node shape function evaluated at $\vec{x}$, and $\hat{u}_i$ is the associated nodal parameter.

Shape function construction

There are a number of schemes to build the shape functions. We have used the Moving Least Squares (MLS) approximation [1],[5]. In the MLS, u^h is expressed as:

$$u^h(\vec{x}) = \sum_{j=1}^{m} p_j(\vec{x}) a_j(\vec{x}) = \boldsymbol{p}^T(\vec{x})\boldsymbol{a}(\vec{x}) \qquad (22)$$

where $\boldsymbol{p}$ is a monomial basis with m terms (e.g. $\boldsymbol{p}(\vec{x}) = [1, x, y]$) and $\boldsymbol{a}$ is a vector of coefficients which are functions of $\vec{x}$. We then build a slightly different approximation, by requiring the monomial basis to be calculated at each node:

$$u^h(x, \vec{x}_i) = \sum_{j=1}^{m} p_j(\vec{x}_i) a_j(\vec{x}) = \boldsymbol{p}^T(\vec{x}_i)\boldsymbol{a}(\vec{x}) \qquad (23)$$

The next step is to define a weighted functional M:

$$M = \sum_{i=1}^{N} w\left(\frac{\|\vec{x} - \vec{x}_i\|}{d_i}\right)[u^h(\vec{x}, \vec{x}_i) - \hat{u}_i]^2 \qquad (24)$$

or

$$M = \sum_{i=1}^{N} w\left(\frac{\|\vec{x} - \vec{x}_i\|}{d_i}\right)\left[\sum_{j=1}^{m} p_j(\vec{x}_i) a_j(\vec{x}) - \hat{u}_i\right]^2 \qquad (25)$$

where d_i is the size of the influence domain associated to node i and w is a function with compact support centered in node i. We have chosen it to be a cubic spline [1]:

$$w = \begin{cases} 2/3 - 4r^2 + 4r^3 & , 0 \le r \le 0.5 \\ 4/3 - 4r + 4r^2 - 4/3\, r^3 & , 0.5 < r \le 1 \\ 0 & , r > 1 \end{cases} \qquad (26)$$

where $r = \|\vec{x} - \vec{x}_i\|/d_i$. Looking for the coefficients a_j that minimize the functional, we have imposed

$$\frac{\partial M}{\partial \boldsymbol{a}} = 0 \qquad (27)$$

After some matrix manipulation, we obtain

$$\boldsymbol{a}(\vec{x}) = [\boldsymbol{A}(\vec{x})]^{-1}[\boldsymbol{B}(\vec{x})]\boldsymbol{u} \qquad (28)$$

where

$$\boldsymbol{u}^T = [\hat{u}_1, \hat{u}_2, \ldots, \hat{u}_N] \qquad (29)$$

$$\boldsymbol{A}(\vec{x}) = \boldsymbol{P}^T\boldsymbol{W}(\vec{x})\boldsymbol{P} \qquad (30)$$

$$\boldsymbol{B}(\vec{x}) = \boldsymbol{P}^T\boldsymbol{W}(\vec{x}) \qquad (31)$$

which are given in terms of $\boldsymbol{P}$ and $\boldsymbol{W}$:

$$\boldsymbol{P} = \begin{bmatrix} p_1(\vec{x}_1) & \cdots & p_m(\vec{x}_1) \\ \vdots & \ddots & \vdots \\ p_1(\vec{x}_N) & \cdots & p_m(\vec{x}_N) \end{bmatrix} \qquad (32)$$

$$\boldsymbol{W}(\vec{x}) = \begin{bmatrix} w\left(\frac{\|\vec{x} - \vec{x}_1\|}{d_1}\right) & \cdots & 0 \\ \vdots & \ddots & \vdots \\ 0 & \cdots & w\left(\frac{\|\vec{x} - \vec{x}_N\|}{d_N}\right) \end{bmatrix} \qquad (33)$$

By equating the expressions (21) and (22) the shape functions are readily available:

$$\boldsymbol{\Phi}(\vec{x}) = [\phi_1(\vec{x}), \ldots, \phi_N(\vec{x})] = \boldsymbol{p}^T\boldsymbol{A}^{-1}(\vec{x})\boldsymbol{B}(\vec{x}) \qquad (34)$$

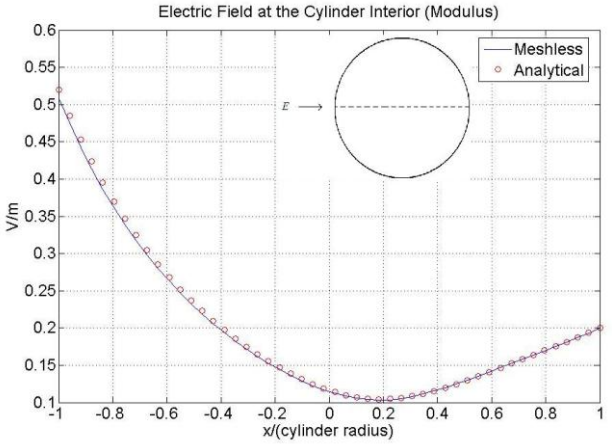

Figure 4. Electric field calculated along the dashed line (modulus). Dimension x normalized with respect to the cylinder radius.

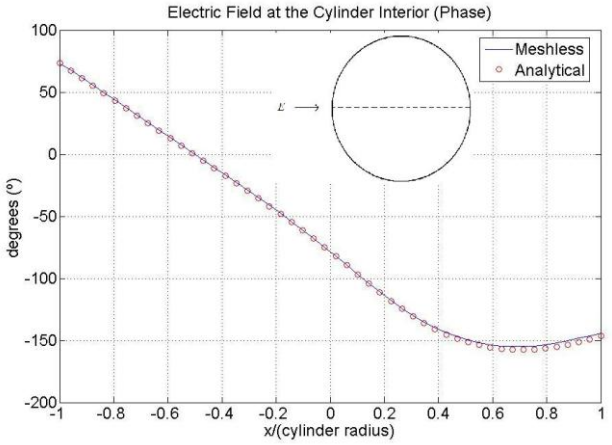

Figure 5. Electric field calculated along the dashed line (phase). Dimension x normalized with respect to the cylinder radius.

IV. DISCRETIZATION AND NUMERICAL IMPLEMENTATION

We begin by spreading nodes over the domain Ω and its global boundary Γ. Then, the total field at any given point $\vec{x}$ inside Ω (or at the boundary Γ) is expressed as a sum of shape functions associated to each node whose influence domain extends over $\vec{x}$:

$$E_z(\vec{x}) = \sum_{I=1}^{N} \phi_I(\vec{x})\hat{u}_I \qquad (35)$$

where N is the number of nodes which influence point $\vec{x}$. To find the nodal parameters $\hat{u}_I$, we enforce the LBIE (18) at each node. The overall procedure is then:

First: Take each node and determine its local domain, verifying if it intersects the global boundary;

Second: Carry out the integrals described in (18). To each node $\vec{x}_i$, evaluate which other nodes influence its local domain.

Third: Assemble in a matrix the interactions between pair of nodes and solve the resulting linear system.

Once the nodal parameters are found, the total field E_z can be calculated everywhere in the domain through application of (35). To verify the precision of the method, we have applied it to the scattering analysis of a plane wave by a dielectric circular cylinder, a problem which is known to possess analytical solution [7]. The global boundary is a circumference located at a distance 1,5 times greater than the cylinder radius. Fig. 3 shows a typical shape function associated to a node located at the origin. The results we have gotten are very precise, which can still be improved by adding more nodes and/or refining the numerical integration schemes.

Figures (4) and (5) show the amplitude and phase for the scattering of a plane wave having unit amplitude by a circular dielectric cylinder of radius $\lambda/2\pi$ and relative permittivity $\varepsilon_r = 2 - j10$ (complex permittivity, which simulates a lossy dielectric).

The total electric field E_z has been calculated along the dashed line that passes through the cylinder center (0,0). Approximately 300 nodes have been spread over the domain Ω (considering its boundary Γ).

V. CONCLUSIONS

We have applied the LBIE method together with a meshless approach to the scattering analysis of a plane wave by a circular dielectric cylinder. The results we have gotten are very precise, and present an excellent agreement when compared to the analytical solution. The meshless LBIE method proved to be a good alternative to FEM; both methods have the feature of producing sparse matrices (as expected from differential formulations), but the latter requires a mesh generation, which is completely unnecessary in the first. The LBIE method is truly meshless; unlike EFG, it does not demand a background grid for integration purposes. Besides that, the RBC's are directly imposed in the formulation. As a drawback, there is much effort to calculate the shape functions numerically at each point, a procedure that is otherwise direct in FEM.

REFERENCES

[1] G. Liu, Mesh Free Methods: Moving Beyond the Finite Element Method, CRC Press, 2002.

[2] G. Parreira, E. Silva, A. Fonseca, and R. Mesquita, "The Element-free Galerkin Method in 3-Dimensional Electromagnetic Problems", *IEEE Transactions on Magnetics*, vol. 42, no. 4, pp. 711-714, 2006.

[3] O. Bottauscio, M. Chiampi, and A. Manzin, "Element-free Galerkin method in eddy-current problems with ferromagnetic media", *IEEE Transactions on Magnetics*, vol. 42, no 5, pp. 1577-1584, 2006.

[4] A. Manzin, and O. Bottauscio, "Element-free galerkin method for the analysis of electromagnetic-wave scattering", *IEEE Transactions on Magnetics*, vol. 44, no 6, pp. 1366-1369, 2008.

[5] S. N. Atluri and S. Shen, " The Meshless Local Petrov-Galerkin Method: A simple & less-costly alternative to the finite-element and boundary element methods", CMES, vol. 3, no 1, pp 11-51, 2002.

[6] A. Peterson, S. Ray, and R. Mittra, *Computational Methods for Electromagnetics*, IEEE Press, 1998.

[7] C. Balanis, *Advanced Engineering Electromagnetics*, John Wiley & Sons, 1989.